Delft University of Technology

3D Carotid Artery Flow Imaging Using Compressive Sensing with a Spatial Coding Mask
A Simulation Study

Hu, Yuyang ; Doğan, Didem; Brown, Michael ; Bulot, Mahé ; Ferin, Guillaume ; Leus, Geert; Kruizinga, Pieter; Steen, Antonius F.W.; Bosch, Johannes G.

Citation (APA)

Important note
To cite this publication, please use the final published version (if applicable).
Please check the document version above.

3D Carotid Artery Flow Imaging Using Compressive Sensing with a Spatial Coding Mask: A Simulation Study

Yuyang Hu[1], Didem Dogan[2], Michael Brown[3], Mahé Bulot[4], Guillaume Ferin[4],
Geert Leus[2], Pieter Kruizinga[3], Antonius F.W. van der Steen[1], Johannes G. Bosch[1]
Email: y.hu@erasmusmc.nl, D.DoganBaskaya-1@tudelft.nl, m.brown@erasmusmc.nl, m.bulot@vermon.com, g.ferin@vermon.com,
g.j.t.leus@tudelft.nl, p.kruizinga@erasmusmc.nl, a.vandersteen@erasmusmc.nl, j.bosch@erasmusmc.nl
[1]Cardiology, Thorax Biomedical Engineering, Erasmus MC, Rotterdam, the Netherlands
[2]Signal Processing Systems (SPS), Delft University of Technology, Delft, the Netherlands
[3] Neuroscience, Erasmus MC, Rotterdam, the Netherlands
[4] Active Probe Group, Innovation Department, Vermon S.A., Tours, France

Abstract— **It has been previously demonstrated that applying an aberrating mask for 2D compressive imaging using a low number of sensors (elements) can significantly improve image resolution, as evaluated via the point spread function. Here we investigate the potential to apply a similar approach for 3D flow monitoring. We conducted a 3D k-Wave simulation using a 5x5 sensor array coupled to a physical coding mask, performing B-mode and power Doppler imaging on a 3D carotid artery flow model. An approximately three times smaller lateral PSF was achieved at the cost of increased background clutter level and slightly increased axial PSF. A better definition of the vessel border and finer flow speckle were observed in power Doppler imaging. Our results suggest that 3D compressive imaging using a very low sensor count of 25 with spatial coding mask has the potential to monitor 3D carotid artery flow.**

Keywords— Compressive imaging, matched filtering, 3D image reconstruction, carotid artery, simulation

I. INTRODUCTION

The carotid artery (CA) is highly accessible for noninvasive ultrasound examination and valuable for cardiovascular health diagnostics or monitoring; e.g., information on blood velocities, wall pulsatility, pulse wave velocity (PWV), and development of atherosclerosis can be assessed [1]. Examination of the complex 3D structure of the CA currently must be performed by a skilled ultrasonographer. For functional monitoring purposes and assessment by unskilled personnel, we aim at a simple, wearable solution with a low number of sensors but inherent 3D capabilities.

Developments in compressive sensing [2] have shown that important information can often be extracted with a surprisingly low number of sensors and observations, seemingly surpassing assumed Nyquist sampling rates. In previous work [3], we have shown that 3D ultrasound image reconstruction is even possible with a single sensor equipped with an aberration mask that provides a spatial coding of the ultrasound field and a model-based reconstruction approach. Furthermore, we have evaluated the possibility of 2D imaging intended for the CA with a low number of sensors with masks [4] and demonstrated

experimentally that a reasonable B-mode image quality could be achieved with only 10 to 12 sensors.

In the current study, we show numerically that an analogous approach can also be applied for 3D imaging and flow sensing of the CA. We simulate a 2D array with a very low number of large elements and an aberration mask. The capability of this array to form volumetric B-mode and power Doppler images, with and without the aberration mask, is evaluated on *in-silico*

a) System scheme
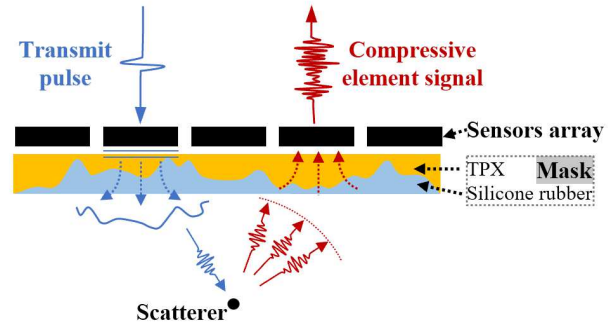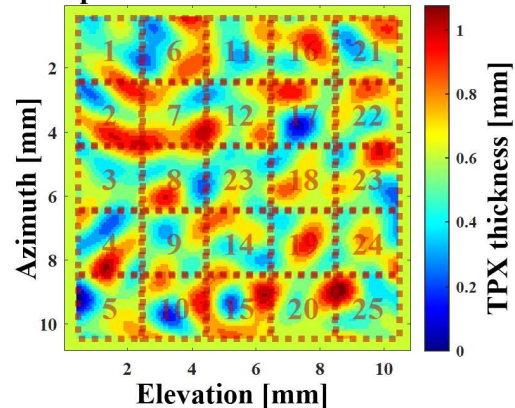

b) Mask pattern

Fig. 1. a) System scheme of compressive imaging with coding mask, with signal path of one transmit/receive sensor pair; b) 5x5 matrix coding mask pattern

TABLE I. PARAMETERS OF K-WAVE SIMULATION

Parameters	Nx (dx) [mm]	Ny (dy) [mm]	Nz (dz) [mm]	Nt (dt) [us]
Grid definition	10 (0.077)	10 (0.077)	26 (0.077)	39 (0.017)

| Medium	Point scatterers model		Flow model		Mask	
	background	scatterers	tissue	blood	TPX	silicone rubber
Speed of sound (std) [m/s]	1540 (-)	1540 (-)	1540 (1.4)	1584 (0.1)	2190 (-)	884 (-)
Density (std) [kg/m^3]	1000 (-)	2000 (-)	1000 (1.4)	1060 (0.1)	830 (-)	1520 (-)
Attenuation [dB/MHz/cm]	0.0022				1.2	10.1

Fig. 2. Point scatterers model reconstruction, shown as maximum intensity projections. a) spatial distribution of scatterers (ground truth) marked by red dots; b) Reconstructed volume projections without the mask (35 dB); c) Reconstructed volume projections with the mask (35 dB)

phantoms: a point scatterers model and a CA-like flow model. Images are reconstructed using a model-based reconstruction approach, and the impact of the aberration mask on the image quality is evaluated.

II. METHODS

A. Transducer and mask

The transducer modeled was a 5x5 square sensor array with a 2x2 mm element pitch and a center frequency of 5 MHz. Since the sensor pitch was almost 7 wavelengths ($\lambda{\sim}0.3$ mm), the imaging region was heavily spatially undersampled. The aperture of 10x10mm was small for carotid imaging but sufficient for proof of principle and was kept limited due to time and memory constraints. All simulations were carried out using the k-Wave toolbox [5]. The simulation setup is shown in Table I. The grid spacing was set to 1/4 wavelength. The coding mask covering the array was formed from layers of two materials with differing sound speeds. The materials chosen were TPX and Silicone rubber, the acoustic properties of which are shown in Table I. The thickness of the two layers is locally varied to generate a spatially varying time delay to the field transmitted by each element. This generates chaotic aberrations and increases the divergence of the element fields (Fig. 1a). Thus, the overlap between different sensors' acoustic fields is enlarged, and the generated coded acoustic fields result in a unique pulse-echo response from each spatial position/imaging voxel. The map of thickness variation (Fig. 1b) was randomly generated to cover a delay range corresponding to 8 wavelengths and then spatially smoothed to keep local gradients smaller than 54° to avoid internal reflections at the interface.

B. In-silico models

Two *in-silico* models were constructed to evaluate the device capabilities: a point scatterer model and a flow model. In the point scatterer model (Fig. 2a), 27 scatterers (1 scatterer per voxel) were firstly evenly distributed in a 10x10x10 mm³ volume centered on the array at a depth of 15 mm and then randomly offset in a small range (<0.4 mm) in each dimension to get some position variability. The background medium properties were set to be similar to those of water (1000 kg/m³, 1540 m/s), while the scatterer density was twice as high (2000 kg/m³). In the flow model (Fig. 3a), which mimics the anatomy
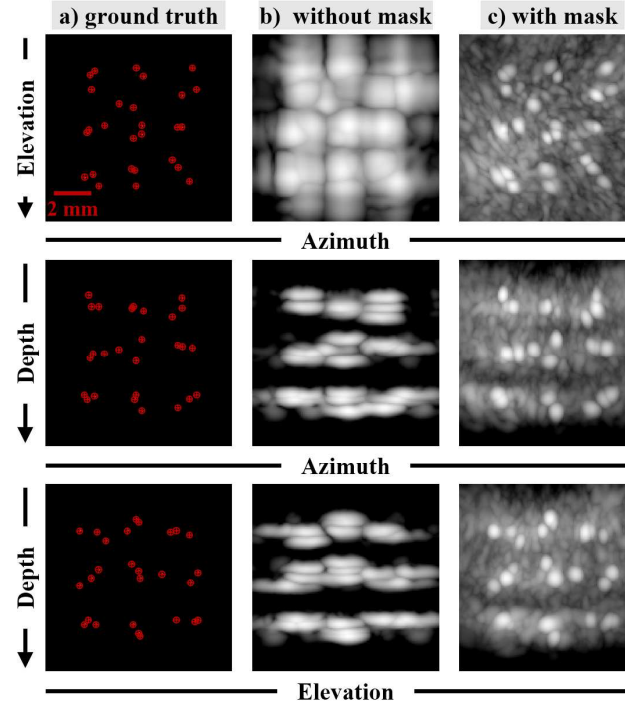
of the carotid artery, a 5 mm diameter cylindrical structure was positioned at 15 mm depth in the azimuth direction of the sensor array and tilted 10° in the elevation and depth direction. The medium properties inside the cylinder were set to those of blood (1060 kg/m³, 1584 m/s), both with a Gaussian variance ($\sigma^2 = 0.1$) to generate weak backscatter. Outside of the cylinder, the medium properties were set to those of human tissue (1000 kg/m³, 1540 m/s), both with a larger Gaussian variance $\sigma^2 = 1.4$). Starting from the initial random distribution, blood scatterers moved under a parabolic flow velocity pattern with a peak velocity of 0.5 m/s. For each volume, new medium properties of each grid voxel were calculated by linear interpolation from the displaced scatterers' properties.

C. System model

A linear model was adopted to describe this imaging system: $y = A \cdot x$, where y represents the vector of RF signals of each sensor (element + mask), x represents the scattering intensity at each position in the volumetric region of interest (ROI), and A is a large matrix containing the pulse-echo impulse responses for each voxel in the ROI for each transmission-reception element pair. The received sensor RF signal is modeled as a sum of impulse responses originating from the scatterers inside the simulated ROI. In this study, we simulated a synthetic aperture transmission scheme for which each element was sequentially excited, and the back-scattered echoes were recorded across all elements. This was chosen to maximize the information the array could acquire. The model for this synthetic aperture transmission scheme was thus structured as follows:

$$\begin{pmatrix} \boldsymbol{y}_{(1,1)} \\ \vdots \\ \boldsymbol{y}_{(t,r)} \\ \vdots \\ \boldsymbol{y}_{(N,N)} \end{pmatrix} = \begin{pmatrix} \boldsymbol{A}_{(1,1)}(1,1,1) & \cdots & \boldsymbol{A}_{(1,1)}(n_x, n_y, n_z) \\ & \ddots & \\ \vdots & \boldsymbol{A}_{(t,r)}(x,y,z) & \vdots \\ & & \ddots \\ \boldsymbol{A}_{(N,N)}(1,1,1) & \cdots & \boldsymbol{A}_{(N,N)}(n_x, n_y, n_z) \end{pmatrix} \begin{pmatrix} \boldsymbol{x}(1,1,1) \\ \vdots \\ \boldsymbol{x}(x,y,z) \\ \vdots \\ \boldsymbol{x}(n_x, n_y, n_z) \end{pmatrix} \quad (1)$$

Each pair of transmitting and receiving sensors has its unique submatrix $\boldsymbol{A}_{(t,r)}$, where t refers to the transmitting sensor, r to the receiving sensor, and N is the number of sensors. Using the reciprocity theorem, the $\boldsymbol{A}_{(t,r)}$ matrix was derived by convoluting the transmitting and receiving sensors' forward fields. For the numerical studies reported here, these forward fields were directly obtained from the k-Wave simulation. For a physical transducer with a mask, these forward fields would be calibrated experimentally. $\boldsymbol{A}$ is considered to be time-invariant. Note that the vector $\boldsymbol{x}$ corresponding to the scatterer intensity of all pixels in the ROI can be time-varying (e.g., in the case of flow or tissue motion), and the corresponding sensor signals $\boldsymbol{y}$ represent $\boldsymbol{x}$ at this time point.

D. Reconstruction method

Image reconstruction concerns deriving the scatterer distribution $\boldsymbol{x}$ in the ROI from the measured element signals $\boldsymbol{y}$, so theoretically, the reconstruction problem is a pseudo-inverse problem of the forward system linear model: $\hat{\boldsymbol{x}} = \boldsymbol{A}^\dagger \cdot \boldsymbol{y}$. Since $N^2 \ll (n_z \times n_y \times n_z)$, the problem is extremely ill-posed and, therefore, intractable for a regular matrix inversion method. We applied a matched filtering method instead, where $\boldsymbol{A}^H$, the Hermitian matrix of $\boldsymbol{A}$ was used as a substitution for $\boldsymbol{A}^\dagger$ [6]:

$$\hat{\boldsymbol{x}}_{MF} = \sum_t^N \sum_r^N \left(\boldsymbol{A}_{(t,r)}^H \boldsymbol{y}_{(t,r)} \right) \quad (2)$$

where each sensor signal $\boldsymbol{y}_{(t,r)}$ was reconstructed individually and accumulated into the final $\hat{\boldsymbol{x}}_{MF}$, In this study $\hat{\boldsymbol{x}}_{MF}$ was

directly used as the estimate of the B-mode image. The estimate $\hat{\boldsymbol{x}}$ might be further improved by a regression-based iterative reconstruction method like LSQR, as we have shown in our previous work [4].

E. Evaluation

In this simulation study, the transducer was driven by a 5 MHz 4 cycles Gaussian pulse with a PRF of 20 kHz, and we investigated the imaging ability of this system with and without the spatial coding mask. The sensor signals corresponding to the *in-silico* models being imaged by the array could have been generated in k-Wave, but this proved to be impractical (would require 31,250 separate time-consuming simulations). Therefore, the sensor signals were generated here by applying the forward model $\boldsymbol{y} = \boldsymbol{A} \cdot \boldsymbol{x}$, where the $\boldsymbol{A}$ matrix was developed from k-Wave sensor pair responses, and $\boldsymbol{x}$ contained the medium acoustic impedance (product of density and speed of sound) for the aforementioned point scatterer or flow model. We verified for a number of exemplary cases (point scatterers, tissue sample distributions) that these model-generated sensor signals were highly similar to the k-Wave simulated signals, even though our forward model ignores multiple-scattering effects. With respect to signal generation for the time-varying flow model, we just needed to update $\boldsymbol{x}$ volume by volume.

After generating the sets of sensor signals for our synthetic transmit aperture scheme, the corresponding volumetric B-mode image $\hat{\boldsymbol{x}}_{MF}$ was reconstructed as described in equation 2.

The B-mode image of the point scatterers model was used to evaluate spatial resolution by analyzing the 27 3D point spread functions (PSF). Except for visually checking the maximum intensity projection in all three dimensions (azimuth, elevation, and depth), every PSF's full width at half maximum (FWHM) in 3D was also measured. Moreover, the average intensity of PSFs (in the FWHM region) was compared to the average intensity of
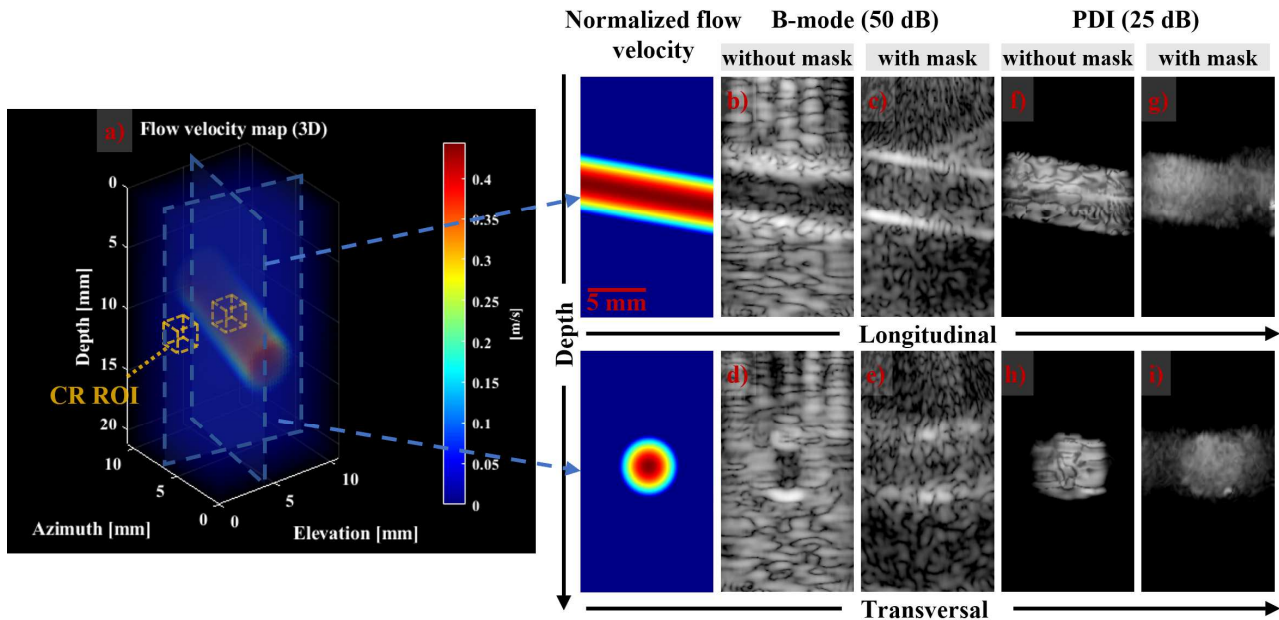

Fig. 3. Flow model reconstruction, shown as cross-sectional images along longitudinal and transversal planes. a) ground truth velocity in volume with ROIs for blood to tissue contrast ratio and cross-sectional velocity images on the right; b~e) cross-sectional B-mode images without and with mask; f~i) cross-sectional power Doppler images without and with mask

the background to calculate the contrast ratio (CR_{SB}). Regarding the flow model, 50 volumes were reconstructed. The static tissue and clutter signal in the B-mode was filtered out by subtracting the mean in slow time, and from the resulting time-varying signals, a PDI was formed. Two cross sections along the longitudinal and transversal direction of the vessel were visually compared (Fig. 3), and two (2x2x2 mm^3) cubic regions at 15 mm depth inside and outside the vessel lumen were selected to calculate the blood to tissue contrast ratio (CR_{BT}).

III. RESULTS

A. Scatterers model

Fig. 2 shows the results of the volumetric reconstructions of the point scatterers model without and with the use of a mask during imaging as a maximum intensity projection (MIP) along three spatial axes with an intensity range of 35 dB. The spatial distribution of scatterers (ground truth) is shown in Fig. 2a. As shown in Fig. 2b, without the coding mask, the scatterers were barely distinguishable and badly localized in the azimuth/elevation MIP (Fig. 2b top image). In the depth direction, the scatterers were still separable. These observations are understandable as without a mask; each sensor works as a single large element generating a narrow vertical A-line, hardly transmitting or receiving energy to/from other spatial locations and elements. The 3D reconstruction, therefore, will resemble a spatial interpolation of 25 individual A-lines.

When using the coding mask (Fig. 2c), both azimuth and elevation PSF were clearly improved. The azimuth FWHM improved from 1.57± 0.2 to 0.55± 0.09 mm and elevation from 1.55± 0.18 to 0.54± 0.08. In the depth direction, the FWHM became slightly larger (from 0.53± 0.05 to 0.65± 0.05 mm).

At the same time, we see a rise of the background clutter level as a side effect of the matched-filtering reconstructions, but not to the level that it obscures scatterer responses. The results confirmed the expected improvement of the PSF at the cost of degradation of CR_{SB} (11.13 to 8.27 dB).

B. Flow model

In the flow model, we performed reconstructions for both volumetric B-mode and PDI (Fig. 3). The ground-truth 3D flow velocity map is shown in Fig. 3a, with 2D cross sections in a longitudinal and transversal plane to the right. The same planes for the B-mode and PDI reconstructions without and with the mask are shown in Fig. 3b-i. In the longitudinal views of the B-mode image, the boundary between blood flow and tissue became sharper and more distinguishable when using the mask (Fig. 3c vs. 3b); however, the CR_{BT} deteriorates (-3.17 to 0.22 dB). These results are in line with those seen in the point scatterer model. This CR_{BT} degradation also explains why the lumen is poorly separable in the transversal image (Fig. 3e). We observe an enhanced flow pattern in the PDI for the reconstruction with the mask (Fig. 3g, 3i). Notably, in the

transversal view, a distinct circular boundary of the flow pattern was reconstructed, which is only slightly affected by the background clutter. Furthermore, the resolution of flow speckles also seems improved. The improved PSF and finer flow speckle may benefit analysis methods such as flow speckle tracking.

IV. DISCUSSION

The current study was limited in several aspects. In this simulation, we only checked the B-mode and PDI imaging performance; other imaging methods, such as color flow Doppler, can also be of interest and will be studied further. Furthermore, a regression-based iterative reconstruction method such as LSQR could improve the reconstruction quality further, as was demonstrated in our previous study [4]. Also, we will test if the finer speckle structure of power Doppler imaging with the mask will allow for flow speckle tracking. Besides, these simulations were performed for a limited aperture size. For a realistic device for CA imaging, a 4-10 times larger aperture area could be used. Due to the large element size, this would still have a manageable number of channels. In the next stage of the project, we will implement this approach experimentally using a real 2D transducer of the same frequency and element pitch and larger aperture manufactured by Vermon S.A., Tours, France, in combination with a physical mask.

V. CONCLUSION

Our results suggest that 3D compressive imaging using a very low sensor count of 25 with a spatial coding mask can potentially image the carotid artery in 3D and monitor 3D carotid artery flow.

REFERENCES

[1] P. M. Nabeel, V. R. Kiran, J. Joseph, V. V. Abhidev, and M. Sivaprakasam, 'Local Pulse Wave Velocity: Theory, Methods, Advancements, and Clinical Applications', *IEEE Rev Biomed Eng*, vol. 13, pp. 74–112, 2020, doi: 10.1109/RBME.2019.2931587.

[2] C. E. Shannon, 'A Mathematical Theory of Communication', *Bell System Technical Journal*, vol. 27, no. 3, pp. 379–423, Jul. 1948, doi: 10.1002/j.1538-7305.1948.tb01338.x.

[3] P. Kruizinga, P. van der Meulen, A. Fedjajevs, F. Mastik, G. Springeling, N. de Jong, J. G. Bosch, and G. Leus, 'Compressive 3D ultrasound imaging using a single sensor', *Sci Adv*, vol. 3, no. 12, Dec. 2017, doi: 10.1126/sciadv.1701423.

[4] Y. Hu, M. Brown, D. Dogan, G. Leus, P. Kruizinga, A. F. W. van der Steen, and J. G. Bosch, 'Compressive Imaging with Spatial Coding Masks on Low Number of Elements: An Emulation Study', in *2022 IEEE International Ultrasonics Symposium (IUS)*, IEEE, Oct. 2022, pp. 1–4. doi: 10.1109/IUS54386.2022.9957699.

[5] B. E. Treeby and B. T. Cox, 'k-Wave: MATLAB toolbox for the simulation and reconstruction of photoacoustic wave fields', *J Biomed Opt*, vol. 15, no. 2, p. 021314, 2010, doi: 10.1117/1.3360308.

[6] G. Turin, 'An introduction to matched filters', *IEEE Trans Inf Theory*, vol. 6, no. 3, pp. 311–329, Jun. 1960, doi: 10.1109/TIT.1960.1057571.